

# Domain State and Temperature Dependence of Pressure Remanent Magnetization in Synthetic Magnetite: Implications for Crustal Remagnetization

Michael W.R. Volk<sup>1,2</sup>, Joshua M. Feinberg<sup>1</sup>

<sup>1</sup>Institute for Rock Magnetism, Department of Earth Sciences, University of Minnesota, 116 Church Street SE, Minneapolis, MN 55455  
<sup>2</sup>Harvard University, Department of Earth and Planetary Sciences, 20 Oxford Street, Cambridge, MA 02138

## Key Points:

- Pressure remanent magnetization (PRM) increases with increasing pressure and decreases with temperature
- The magnitude of the imparted PRM is the same across magnetite grain sizes
- PRM is independent of thermal remanence acquired in the same temperature interval

**Abstract**

Pressure remanent magnetization (PRM) is acquired when a rock is compressed in the presence of a magnetic field. This process can take place in many different environments from impact and ejection processes in space, to burial and subsequent uplifting of terrestrial rocks. In this study, we systematically study the acquisition of PRM at different pressures and temperatures, using synthetic magnetite in four different grain sizes ranging from nearly single-domain to purely multi-domain. The magnitude of the PRM acquired in a  $300 \mu T$  field is, within error, independent of the domain state of the sample. We propose that the acquisition of a PRM is mainly driven by the magnetostriction of the magnetic material. We further show that compared to a thermal remanent magnetization, the acquisition of PRM in large multi-domain grains can be quite efficient, and may represent a significant component of magnetization in low-temperature – high-pressure environments.

**1 Introduction**

Pressure cycling of a rock can have a dramatic influence on the magnetic properties of the minerals that it contains. One phenomenon that has been the focus of many studies recently is the loss of remanence through pressure cycling, where the application of pressure to a rock in a zero-field environment removes parts of the remanent magnetization (Bezaeva, Gattacceca, Rochette, Sadykov, & Trukhin, 2010; Gattacceca, Lamali, Rochette, Boustie, & Berthe, 2007; Louzada, Stewart, Weiss, Gattacceca, & Bezaeva, 2010; Louzada et al., 2011; Volk & Gilder, 2016). The higher the pressure the more remanence is removed. However, on Earth a zero-field environment is rarely the case, as magnetic fields are usually present.

Pressure remanent magnetization (PRM) or piezo remanent magnetization is the magnetic remanence acquired by pressure cycling a sample in a magnetic field (Nagata, 1966). In the late 1960s, the acquisition of PRM under uniaxial compression was investigated intensively (Kinoshita, 1968a, 1968b, 1969; Kinoshita & Nagata, 1967; Nagata & Carleton, 1968, 1969a, 1969b; Nagata & Kinoshita, 1965). However, changes in remanence are extremely sensitive to the degree of hydrostaticity (Volk & Gilder, 2016) and very few data are available for the acquisition in a mostly hydrostatic regime.

Pressure remanent magnetization is important in several environments. PRMs can be acquired during impacts or large collisions, either in extraterrestrial environments or on Earth, in the presence of an ambient field (e.g. dynamo fields, fields in the solar nebula) (Tikoo et al., 2015). In other environments, the overburden of rocks, ice, or water may create hydrostatic pressure, which in the presence of a magnetic field may create a PRM (Dunlop & Özdemir, 1997). However, while the pressure experienced by meteorites often exceeds several GPa (Stöffler, Keil, & Edward R D, 1991), lithospheric pressures are typically much lower ( $< 2\text{GPa}$ ) (Gillen, 1982). In both cases, temperature may also increase which can affect the acquisition efficiency of the PRM.

Paleomagnetic studies rely on a comprehensive understanding of the origin of remanence in order to correctly interpret past processes, such as continental rotations, paleosecular variations and geomagnetic reversals. In paleointensity studies, the isolation of a pure TRM is critical for a robust recovery of the magnetic field strength during the formation of the rock. PRMs have the potential to interfere with paleodirectional and paleointensity studies, in large part because so little is understood about their acquisition and subsequent identification in the lab. Here we investigate the PRM acquisition efficiency of Ti-free magnetite in several grain-sizes / magnetic domain states as a function of pressure ( $< 400 \text{MPa}$ ) and temperature to assess the importance of PRMs in nature for various terrestrial environments.

## 2 Materials and Methods

This study uses four synthetic, commercial (Wright) magnetite powders (4000, 112978, 041183, 112982) of varying grain-size. The magnetic properties of these magnetite powders have been studied previously (e.g. Yu, Dunlop, & Özdemir, 2002; Yu, Dunlop, & Özdemir, 2002), and their mean grain-size has been determined by TEM to be 0.065, 0.44, 18.33 and 16.9  $\mu\text{m}$  for 4000, 112978, 041183, and 112982, respectively (Yu, Dunlop, & Özdemir, 2002). The powders were annealed for 24 hrs at 500°C in CO/CO<sub>2</sub> atmosphere to reduce any low-temperature oxidation that may have occurred during storage. After annealing, the magnetic susceptibility as a function of temperature was measured on a Geophysica Kappabridge KLY-2 (300 Am<sup>-1</sup> field at 920 Hz) for each powder in Ar-atmosphere. The annealed powders (100 mg or 0.5 wt.%) were mixed with Omega CC high temperature cement and cast as solid cylindrical samples of 10 mm diameter and height and cured for 2 days at room temperature.

Hydrostatic pressure cycling of the samples was done with a commercially available 13 mm heated piston type pressure cell from Across International (SDS13.H). To withstand high pressure at elevated temperatures, the material of the cell is hardened steel. Before use, the cell was demagnetized using alternating fields of  $\approx 90$  mT, which resulted in residual fields of  $< 5 \mu\text{T}$ . The pressure was applied using a SpecAC Atlas 25T automatic press. Silicone oil (Sigma Aldrich #378399) was used as the pressure medium. A magnetic field was produced by a set of homemade Helmholtz coils around the cell and monitored before each pressure step ( $300 \pm 28 \mu\text{T}$ ,  $n=145$ ). The samples were placed in a Teflon cup together with the pressure medium. At room temperature, pressure was applied, held for 0.1 min and then released. Both application and release of pressure was done at a slow setting ( $\approx 10$  sec/100 MPa). The PRM experiments at elevated temperatures (80°C, 150°C) were done in a similar fashion. First, the magnetic field was applied while the sample was heated to  $T_h$  ( $\approx 3^\circ\text{C}/\text{min}$ ). After  $T_h$  was reached, the sample was allowed to equilibrate for 15 minutes. Then, pressure was applied and the sample was cooled to room temperature using a fan ( $\approx 2^\circ\text{C}/\text{min}$ ). Each pressure/temperature step was repeated 3 times using the same specimen to ensure reproducibility of the results. Remanent measurements were collected on a 2G U-channel magnetometer in a shielded room with a background field of 100 nT.

Hysteresis loops and direct current demagnetization curves were measured on a Princeton Measurements Vibrating Sample Magnetometer (VSM). In order to maintain the demagnetized state of the samples, sister specimens (denoted by \*) were measured to determine the hysteresis properties before pressurization. The measurements were repeated on the pressurized samples, after the pressure experiments were finished.

Low-temperature measurements consisting of warming of a field cooled (FC, 2.5T) low-temperature saturating isothermal remanent magnetization (LTSIRM) and a zero-field cooled (ZFC) LTSIRM acquired in 2.5T at 10 K were obtained with a Quantum Design Magnetic Property Measurement System (MPMS) on sister specimen before pressure cycling. The LTSIRM were warmed at 5 K/min from 10 K to room temperature in zero-field.

## 3 Results

The Curie temperature of pure (Ti-free) stoichiometric magnetite is  $T_c=575 - 585^\circ\text{C}$  (Dunlop & Özdemir, 1997). We determined  $T_c$  from the negative maximum of the first derivative ( $d\chi/dT$ ) of the susceptibility (table 1) (Fabian, Shcherbakov, & McEnroe, 2013; Petrovský & Kapička, 2006). All samples give Curie temperatures close to the literature value of pure stoichiometric magnetite. Therefore, impurities, such as Ti are minimal, as they typically reduce the Curie temperature.

Magnetite undergoes a crystallographic phase transition (Verwey transition) at  $T_V \approx 120\text{K}$  (Verwey, 1939). The transition is suppressed for magnetite with even small Ti substitutions and sensitive to oxidation (Özdemir, Dunlop, & Moskowitz, 1993; Shepherd, Koenitzer, Aragn, Spalek, & Honig, 1991). Oxidized magnetite shows a less pronounced transition with diminished Verwey temperatures (Özdemir et al., 1993; Shepherd et al., 1991). We calculated  $T_V$  (max  $dM/dT$ ) from the FC and ZFC experiments (fig. 1), after background subtraction (Liu et al., 2003). Most samples yield low Verwey transition temperatures, indicating oxidation or disorder. The exception is sample 041183 ( $18.3\ \mu\text{m}$ ) with a  $T_V$  of 123 K close to the literature value for pure stoichiometric magnetite. Curie temperature and Verwey transition temperature show that the initial powders are magnetite with a varying degree of oxidation or disorder, with 112978 ( $0.44\ \mu\text{m}$ ) being the most and 041183 ( $18.3\ \mu\text{m}$ ) the least oxidized/disordered.

### 3.1 Domain State

Initial measurements showed that the cement samples compact under pressure, resulting in minor changes in volume and magnetic properties. This one time change is expected as pore spaces within the cement are reduced and dislocations are introduced into large magnetite grains. Therefore, to avoid complications in subsequent experiments, we pre-compressed a second batch of samples until no volume change was detectable and the pore spaces removed. Figure 1d illustrates how this initial pre-compaction of the the samples (arrow in fig. 1a) changes their magnetic properties. The remanence ratio ( $M_r/M_s$ ), an indication of domain state, increased for all samples after compaction. Similarly  $B_c$  and  $B_{cr}$  increased, while their ratio ( $B_c/B_{cr}$ ) decreased, indicating more single-domain behavior after compaction. Similar increases in coercivity by pressure cycling were reported in earlier studies (Gilder & Le Goff, 2008; Reznik, Kontny, Fritz, & Gerhards, 2016). The more SD-like behavior is usually attributed to the introduction of stacking faults and dislocations in the magnetite grains, which act as new pinning sites for domain walls (Kontny, Reznik, Boubnov, Göttlicher, & Steininger, 2018; Lindquist, Feinberg, Harrison, Loudon, & Newell, 2015). Consequently, the increased dislocation density increases the coercivity as well as the remanence efficiency of the sample (Dunlop & Özdemir, 1997).

To verify that the magnetic properties did not change during the PRM experiments, we remeasured rock-magnetic properties after completing all P/T cycles (filled markers in fig. 1a and batch 2 in table 2). Comparing the absolute values for  $M_s$  and  $M_{rs}$  between batch #1 and #2 is misleading as their magnetite content is subtly different. However, the coercivity ( $B_c$ ) and coercivity of remanence ( $B_{cr}$ ), as well as the remanence and coercivity ratios are independent of magnetite concentration and can be used to assess possible changes. While the initial compaction led to a significant change in magnetic properties, the 16 additional pressure/temperature cycles had little effect (fig. 1a). Therefore, we are confident that the magnetic mineral assemblage remained stable during the P/T experiments.

Figure 1d, shows the so called "squareness plot" (Wang & Van der Voo, 2004), which can be used to estimate the domain state and Ti-content of magnetite. Samples with a squareness ( $M_{rs}/M_s$ ) below 0.05 and low coercivities are generally considered multi-domain (Day, Fuller, & Schmidt, 1977; Dunlop, 2002). Ti rich samples are shifted to the left of the "Ti-free" line, towards lower  $B_c$  values (Wang & Van der Voo, 2004). The four samples show a nice progression from multi-domain ( $16.9\ \mu\text{m}$ ) to more single-domain ( $0.065\ \mu\text{m}$ ) behavior. Furthermore, Ti-substitutions must be minimal or absent, since all samples show higher  $B_c$  values than expected for Ti substituted magnetite (Wang & Van der Voo, 2004). Instead, all samples show evidence of either minor oxidation or increased coercivity related to their initial composition.

First order reversal curve (FORC) diagrams are a useful tool to assess the distribution of domain states within a sample. The FORC diagrams (fig. 1c,d) for the two smallest grain-sizes (0.065 & 0.44  $\mu\text{m}$ ) show a wide, closed distribution of  $B_c$  values along  $B_u = 0$ . Furthermore, the 0.065  $\mu\text{m}$  sample shows a small negative region for negative  $B_u$  values, as would be expected for non-interacting single-domain grains. Both 0.065  $\mu\text{m}$  & 0.44  $\mu\text{m}$  have a pronounced teardrop shape with interaction lobes that are indicative of strongly interacting SD particles. This may be an indication that grains of magnetite were not homogeneously dispersed throughout the cement, and that portions of the magnetite assemblage may be interacting. Such a scenario would also explain the relatively low  $M_{rs}/M_s$  observed here. We interpret these two finest grain samples as being dominated by interacting SD and vortex state domains (Harrison & Lascu, 2014; Roberts, Heslop, Zhao, & Pike, 2014). The large positive distribution of the 0.065  $\mu\text{m}$  sample is located at higher  $B_c$  values indicating a more SD state than the 0.44  $\mu\text{m}$  sample, which is further supported by the higher remanence ratio. The larger grains 16.9  $\mu\text{m}$  and 18.3  $\mu\text{m}$  (fig. 1e,f), have a peak in their coercivity distributions at much lower  $B_c$  values, near the origin. This shows a more multi-domain behavior compared to the other samples (Roberts et al., 2014). However, even for these larger grains, a small but noticeable high coercivity component is visible, similar to that observed in MD magnetite in Lindquist et al. (2015). This is likely caused by a wide distribution of grain sizes that range into smaller vortex state grains as well as internal strain left behind from the annealing process cooling.

The multi-domain character of the 16.8  $\mu\text{m}$  and 18.3  $\mu\text{m}$  samples is further supported by the warming of the low-temperature SIRM acquired in a 2.5 T field at 10 K. Large multi-domain particles, have a smaller moment after field cooling (1a solid line) than after zero-field cooling (1a dashed line) (Carter-Stiglitz et al., 2006). Both multi-domain samples (16.9 & 18.3  $\mu\text{m}$ ), before and after compression, show this behavior (see also Carter-Stiglitz et al., 2006), while the smaller vortex dominated samples (0.065 & 0.44  $\mu\text{m}$ ) show the opposite. Finally, the FORC diagrams (fig. 1c-f), squareness plot (fig. 1b) and low-temperature magnetization behavior show that the samples can be ordered according to their domain state from smallest (SD) to largest (MD) (0.065, 0.044, 18.3, 16.9  $\mu\text{m}$ ), in agreement with the TEM observations of Yu, Dunlop, and Özdemir (2002).

### 3.2 Pressure Remanence

A magnetization acquired at ambient temperature ( $T_0$ ) and pressure ( $M(T_0, P_0)$ ) in a magnetic field (300 $\mu\text{T}$ ) is an isothermal remanent magnetization (table 2). All samples acquire a small  $M(T_0, P_0)$ , on the order of 0.01-0.03  $\text{mA}\cdot\text{m}^2/\text{kg}$ . When the samples are pressure cycled in the same magnetic field, they acquire a PRM. The PRM is at least one order of magnitude larger than  $M(T_0, P_0)$  even at the lowest pressure ( $\approx 200$  MPa) and increases with pressure (fig. 2a). Interestingly, all samples acquire a PRM of roughly (within error) the same magnitude (black marker in fig. 2d).

The zero pressure remanence ( $M(T_h, P_0)$ ) acquired at  $T_h = 80^\circ\text{C}$  (fig. 2b) and  $T_h = 150^\circ\text{C}$  (fig. 2c) is a partial thermal remanence (pTRM). By cooling from  $T_h$ , grains with blocking temperatures ( $T_B < T_h$ ) acquire a magnetization  $M(T_h, P_0)$ . The most multi-domain samples (16.9 & 18.3  $\mu\text{m}$ ) acquire the lowest pTRM, the finer-grained vortex samples acquire a greater pTRM (tab. S2). Similarly, the PRM at elevated temperatures increases with increasing temperature and pressure. Furthermore, the PRM at temperature shows a similar domain-state dependence as the pTRM.

## 4 Discussion

The absolute values for the PRM acquired by pressure cycling in a magnetic field at room temperature seem, within error, independent of the domain state of the

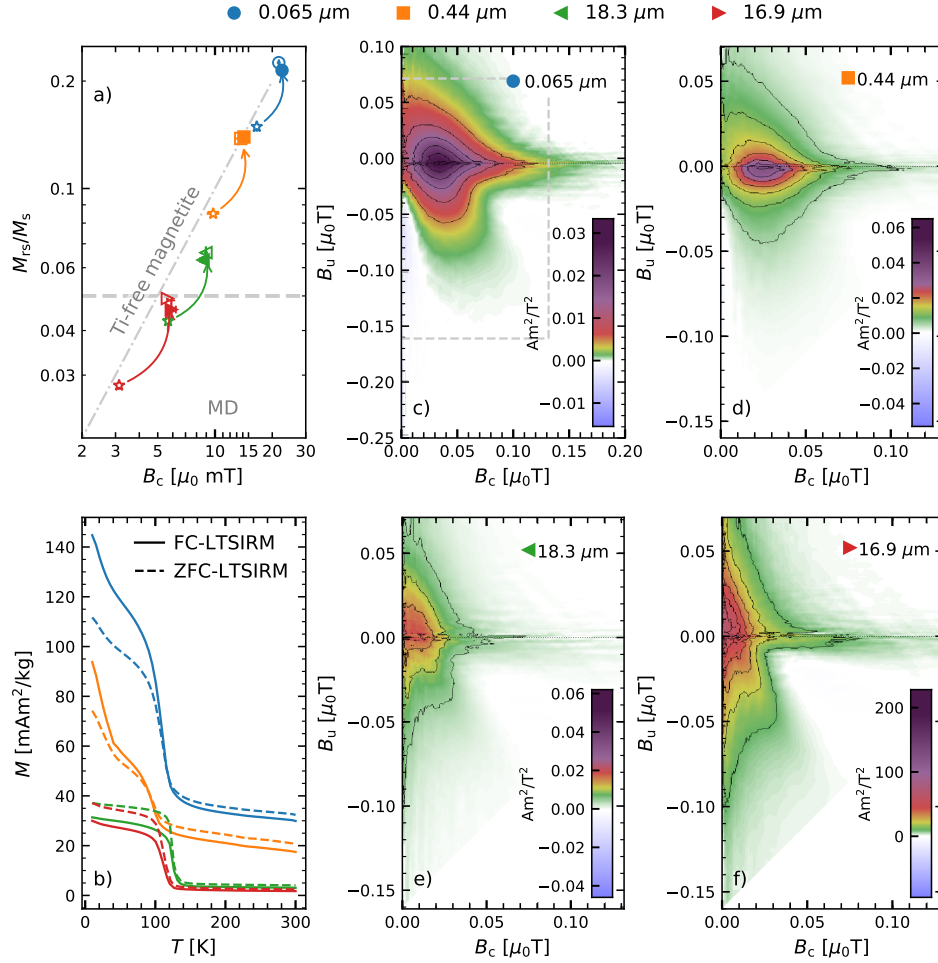


**Figure 1.** Rock magnetic properties of magnetite samples. **a)** Squareness plot showing changing magnetic properties after compaction. Stars show samples before pre-compression, arrows point to samples post-compression. Open and filled symbols show samples before and after compaction and subsequent P/T experiments, respectively. The observation that the hysteresis properties immediately after the compaction are so similar to those after all subsequent P/T experiments shows that the magnetic mineral assemblage was stable throughout the course of this study. Slanted dashed line corresponds to Ti-free magnetite line from Wang and Van der Voo (2004). Dashed horizontal line corresponds to multi-domain line from Day et al. (1977). **b)** Mass normalized low-temperature remanence (10 K) after FC (solid line) and ZFC (dashed line) of the pre-compressed samples as a function of temperature. **c-f)** FORC diagrams for the magnetite (0.5 wt. %) samples in Omega CC high temperature cement calculated using the VariFORC method (Egli, 2013) implemented in FORCinel (Harrison & Feinberg, 2008) with smoothing factors of  $Sc_0 = Sb_0 = 4$ ,  $Sc_1 = Sb_1 = 6$ , and  $\lambda = 0.1$ . Note different  $B_c, B_u$  axis in **c)**. Dashed box in **c)** shows extent in **d-f)** for comparison.

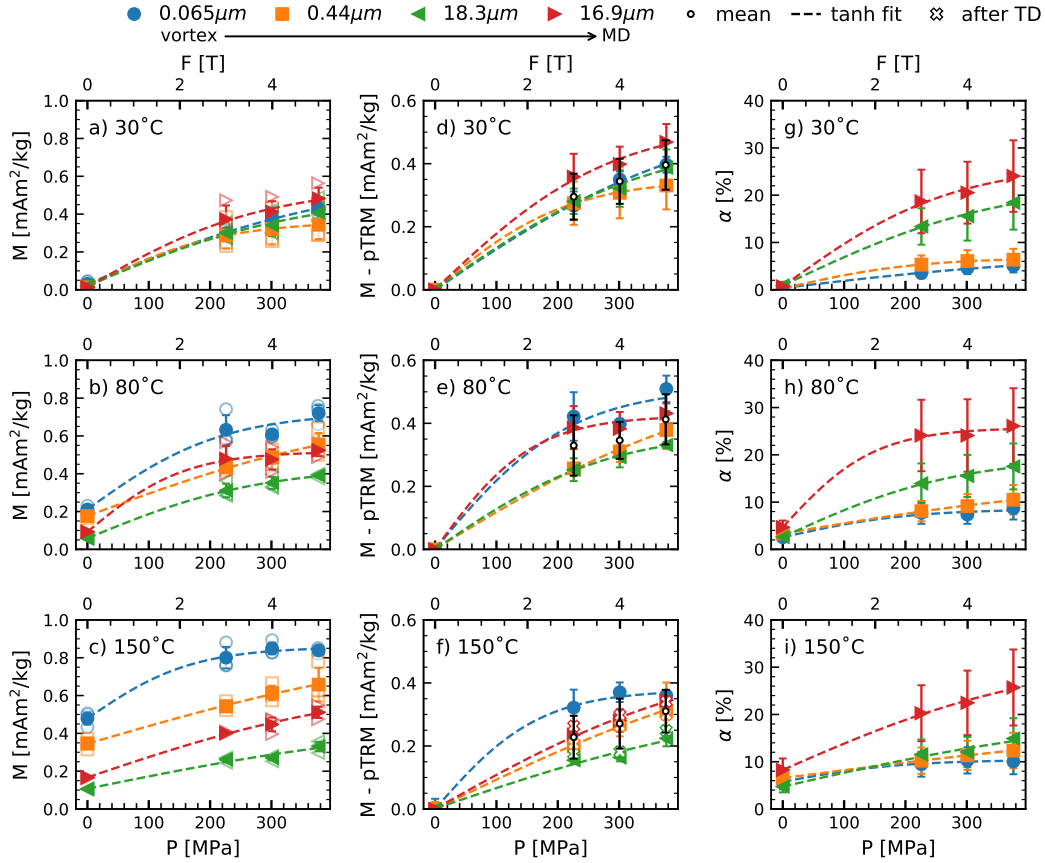


**Figure 2.** Magnetic moment acquired in 300  $\mu\text{T}$  field as a function of force [T] / pressure [MPa] for magnetite in four different grain-sizes at 30°C, 80°C and 150°C. Left column (a-c) show magnetic moment as measured, the nature of the moment (PRM; PRM+pTRM ...) depends on P/T conditions (see text). Center column (d-f): PRM after subtraction of the isothermal/viscous remanence (d) or pTRM(T,  $P_0$ ) (e,f). Crosses mark PRM after thermal demagnetization (TD) to 150°C in zero-field. Right column (g-i): strength of the PRM relative to a TRM as estimated by REM method ( $\alpha = \text{PRM}/\text{TRM}$  in %). Black open marker in d,e,f show the mean for all samples with one standard deviation uncertainty.

**Table 1.** Magnetic properties before and after pressure cycling. Batch 1\* denotes samples before any compaction, batch 1 denotes samples after initial compaction, and batch 2 denotes a second set of samples after all of the P/T treatments in this study. Uncertainties correspond to one standard deviation with  $n(1^*)=12$ ,  $n(2)=4$ .

sample	batch	$T_C$ [°C]	$T_V$ [K]	$M_s$ [mAm <sup>2</sup> /kg]	$M_{rs}$ [mAm <sup>2</sup> /kg]	$B_c$ [mT]	$B_{cr}$ [mT]	$M_{rs}/M_s$	$B_{cr}/B_c$
0.065 $\mu\text{m}$	1*	590	114	488.3±49.3	72.9±8.8	16.6±0.5	40.3±1.9	0.15	2.4
	1		112	413	93.0	21.6	43.5	0.23	2.0
	2			391.7±6.3	83.9±1.3	22.5±0.3	46.6±0.7	0.21	2.1
0.44 $\mu\text{m}$	1*	575	96	464.9±13.8	39.5±1.5	9.8±0.8	34.4±2.1	0.09	3.5
	1		96	420	58.0	13.7	36.1	0.14	2.6
	2			386.5±7.5	53.9±2.2	14.2±0.5	37.9±0.4	0.14	2.7
18.3 $\mu\text{m}$	1*	592	123	379.0±11.1	16.1±0.9	5.7±0.2	26.4±0.6	0.04	4.7
	1		124	363	24.0	9.0	28.4	0.07	3.2
	2			357.6±7.6	22.5±0.4	8.7±0.1	28.7±0.1	0.06	3.3
16.9 $\mu\text{m}$	1*	590	113	426.2±15.8	12.0±0.3	3.1±0.1	20.2±0.7	0.03	6.5
	1		112	427	21.0	5.6	22.4	0.05	4.0
	2			452.9±109.3	20.5±3.2	5.9±0.4	24.5±0.3	0.05	4.2

**Table 2.** Remanent magnetization at different temperatures in mAm<sup>2</sup>/kg. Standard deviation was calculated from 3 separate P/T cycles of the same specimen.  $M(T, P)$  is the average for all samples without subtracting the pTRM ( $M(T, P_0)$ ),  $\Delta M(T, P)$  is the mean after subtraction.

P [MPa]	T [°C]	0.065 $\mu\text{m}$ [mAm <sup>2</sup> /kg]	0.44 $\mu\text{m}$ [mAm <sup>2</sup> /kg]	18.3 $\mu\text{m}$ [mAm <sup>2</sup> /kg]	16.9 $\mu\text{m}$ [mAm <sup>2</sup> /kg]	$M(T, P)$ [mAm <sup>2</sup> /kg]	$\Delta M(T, P)$
0	30	0.03±0.02	0.01±0.01	0.02±0.00	0.01±0.00	0.02±0.01	0.00
	80	0.21±0.02	0.18±0.01	0.06±0.00	0.09±0.00	0.13±0.06	0.00
	150	0.43±0.10	0.28±0.12	0.09±0.03	0.14±0.05	0.23±0.15	0.00
226	30	0.30±0.04	0.29±0.07	0.30±0.04	0.37±0.07	0.31±0.07	0.30
	80	0.63±0.08	0.43±0.01	0.31±0.04	0.48±0.07	0.46±0.13	0.33
	150	0.72±0.15	0.46±0.15	0.24±0.04	0.37±0.06	0.45±0.20	0.21
301	30	0.38±0.03	0.32±0.08	0.34±0.06	0.41±0.06	0.36±0.07	0.34
	80	0.61±0.02	0.49±0.03	0.35±0.03	0.48±0.05	0.48±0.10	0.35
	150	0.77±0.14	0.53±0.16	0.25±0.04	0.41±0.07	0.49±0.22	0.26
376	30	0.43±0.03	0.34±0.08	0.41±0.06	0.48±0.06	0.42±0.08	0.40
	80	0.72±0.04	0.56±0.06	0.39±0.01	0.52±0.03	0.55±0.12	0.41
	150	0.76±0.14	0.57±0.17	0.31±0.04	0.47±0.08	0.53±0.19	0.30

sample. At elevated temperatures on the other hand, smaller grains acquired a larger magnetization. However, in contrast to  $M(T_r, P)$ , the remanence acquired by pressure cycling at  $T_h$  is a superposition of the pTRM ( $M(T_n, P_0)$ ) and the PRM. Thus, the "true" PRM can be determined by subtracting the pTRM from  $M(T_n, P)$  (fig. 2d-e). This assumption is only valid if the PRM and the pTRM are independent; meaning, the PRM magnetizes only grains, that are not "remagnetized" by cooling in a field and vice versa. To test this hypothesis, we repeated the PRM acquisition at 150°C for three specimens and demagnetized them thermally to the same temperature. For all specimen, the remanence after thermal demagnetization (crosses in fig. 2f) is close to the values obtained by simple arithmetic subtraction. As a consequence, the PRM is independent of the pTRM at least within this pressure/temperature range, and shows that grains with a blocking temperatures  $T_B > T_h$  are magnetized by pressure

cycling. Tikoo et al. (2015) thermally demagnetized a PRM that was acquired at room temperature. They showed that while the median destructive field of the PRM is low, the thermal stability is greater than would be expected and can reach up to the Curie temperature of the mineral. Thus, the independence of PRM and pTRM is supported by the thermal high stability during thermal demagnetization found by Tikoo et al. (2015). After establishing, that a simple arithmetic subtraction results in a valid value for the PRM at temperature, the PRM values at 80°C and 150°C show little domain-state dependence, similar to the room temperature PRM.

This independence of grain-size is somewhat unexpected. Almost all magnetic properties have some relation to the domain state and/or grain-size of the magnetic particles. For instance, the saturation isothermal remanence of particles is strongly domain-state dependent (e.g. Day et al., 1977). While the pTRM acquisition in our samples shows domain state dependence, our data suggest, that the PRM is independent of the domain state. Consequently, the acquisition mechanism must also be independent of domain state.

Magnetostriction is a physical property of magnetite that is independent of the domain state. Magnetostriction describes a change in the dimension of a crystal as it is magnetized. For magnetite, magnetostriction is a strongly anisotropic quantity and depends on the crystallographic direction ( $\lambda_{100} = -17 \times 10^{-6}$ ,  $\lambda_{111} = +90 \times 10^{-6}$ ) (Bickford, Pappis, & Stull, 1955). Magnetite has an isotropic magnetostriction constant of  $\lambda_s = 43 \times 10^{-6}$ , which increases strongly with Ti substitution (Dunlop & Özdemir, 1997; Moskowitz, 1993). At elevated temperatures,  $\lambda_s$  decreases approximately proportional to  $(1 - T/T_c)^{0.9}$  (Moskowitz, 1993). For the temperatures used in this study,  $\lambda_s(80^\circ\text{C})$  decreases by only  $\approx 4\%$  at 80°C and  $\approx 14\%$  at 150°C (Moskowitz, 1993). In addition, hydrostatic pressure linearly increases the magnetostriction constant by  $\approx 15\%/100$  MPa, however data for  $P > 200$  MPa are not available (Kinoshita & Nagata, 1967; Nagata & Kinoshita, 1967). Fabian (2006) showed that magnetite changes from a cubic anisotropy to stress dominated anisotropy, when  $\approx 20$  MPa of uniaxial compression is applied. While the our experiments were done under hydrostatic stress, it indicates that as pressure is applied, the anisotropy can change and particles can be remagnetized along the applied field direction. The different minerals within a rock have different compressibilities (Hazen, 1985). This, can add shear between grains and may result in a non-hydrostatic component that at hydrostatic pressures much higher than 20 MPa can lead to a similar change in anisotropy. In a single domain case, this change in anisotropy changes the direction of the easy axis, which changes back upon decompression. If a field the magnetization would then be locked preferentially aligned with the applied field direction. Similarly, in the multi-domain case, the domain walls move as the applied pressure changes the anisotropy. When pressure is released, the domain walls move back, being pinned at dislocations creating a non zero magnetization.

Using the temperature and pressure dependence of  $\lambda_s$ , one would expect that increasing pressure would increase the magnitude of the PRM, while a temperature increase would decrease the magnitude. At 80°C the average PRM is about 6% stronger, while it is -21% weaker at 150°C, when compared to the room temperature value. Therefore, the theory seems to be compatible with our data when the uncertainties of the measurements are considered (fig. 3a). A way to test the magnetostrictive influence on the acquisition of PRM, would be to repeat these experiments with materials that have a stronger magnetostriction, such as Ti substituted magnetite (Moskowitz, 1993). Another way would be to change the sequence for applying and releasing field ( $B_+$ ,  $B_-$ ) and pressure ( $P_+$ ,  $P_-$ ) as it should change the PRM intensity. Nagata and Carleton (1969a) have shown that application of  $P$  and  $B$  are not commutative under non-hydrostatic conditions. Thus, a PRM acquired with the protocol presented in this

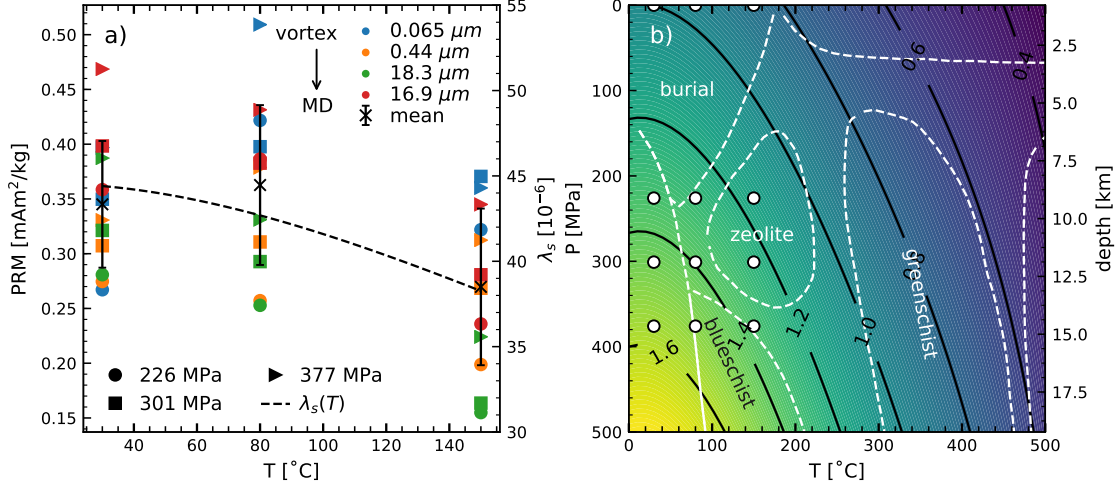


**Figure 3.** **a)** Temperature dependence of PRM acquisition after subtraction of IRM/pTRM moment at zero pressure. Black crosses show the mean for all samples with one standard deviation of uncertainty. Dashed lines denotes the temperature dependence of the saturation magnetostriction constant ( $\lambda_s$ , right y-axis) calculated from 5th order polynomial fit given in Moskowitz (1993). **b)** Temperature and pressure dependence of the saturation magnetostriction constant  $\lambda_s$ , normalized to the room temperature value. Regions for metamorphic facies from Gillen (1982). White dots mark the temperature/pressure pairs explored in this study.

paper ( $B_+P_+P_-B_-$ ), should be larger than when the pressure is released in zero field ( $B_+P_+B_-P_-$ ).

#### 4.1 Comparing PRM to TRM

While high pressure ( $> 1$  GPa) PRM experiments show that a secondary overprint can be recorded (Gattacceca et al., 2007; Tikoo et al., 2015), it remains an open question whether PRMs acquired at crustal pressures ( $< 400$  MPa) can substantially deflect or overprint a specimen’s natural remanent magnetization. The initial powders were mixed with a high temperature cement. While the cement remains solid at high temperatures, its chemical composition changes at temperature above approximately  $400^{\circ}\text{C}$ , likely due to the binding process. Heating to lower temperatures did not show any significant changes in magnetic mineralogy. The cement’s chemical change is likely to also affect the magnetite powders, which makes heating the samples to temperatures  $>400^{\circ}\text{C}$  undesirable. Therefore, to compare the strength of the PRM to a full TRM we use the so-called ratio of equivalent magnetizations (REM) method (Kletetschka, Kohout, & Wasilewski, 2003) to estimate the thermoremanence.

$$M(\text{TRM}) \approx \frac{M_{rs}B_{\text{lab}}}{3000\mu T}$$

Where  $M_{rs}$  is the saturation remanence of the sample (i.e. saturated isothermal remanence) determined from a hysteresis loop and  $B_{\text{lab}}$  is the applied field in  $\mu T$  (i.e.  $300 \pm 28\ \mu T$ ) that the TRM is acquired in. The REM method is frequently used to estimate paleointensity values for meteorites, which, like our samples, cannot be heated (Gattacceca & Rochette, 2004; Tikoo et al., 2014). Here, we adopt the approach of Tikoo et al. (2015) and use this method in reverse to estimate a full TRM.

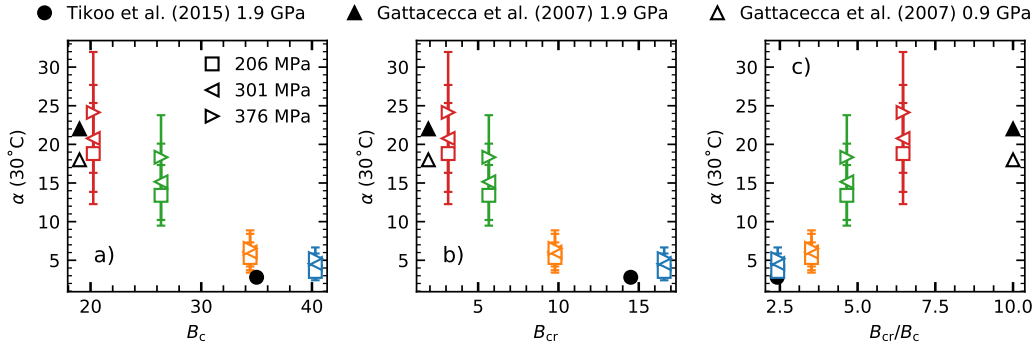


**Figure 4.** PRM efficiency ( $\alpha$ ) at room temperature as a function of **a)** coercivity, **b)** coercivity of remanence, and **c)** remanence ratio. Data from (Gattacceca et al., 2007; Tikoo et al., 2015) of samples containing only Ti-free magnetite after AF demagnetization at 2 mT, for comparison.

To estimate uncertainty we used a bootstrapping approach. For the TRM estimation, we randomly picked 1000 values from a skewed gaussian distribution (mean = 3000, skewness = 1.7) for the uncertainty of the REM method, one value out of the 145  $B_{lab}$  measurements, and the  $M_{rs}$  value determined from hysteresis loops. Furthermore, to get the uncertainty of the PRM efficiency ( $\alpha = \text{PRM}/\text{TRM}$ ), a randomly picked PRM value was divided by the TRM estimation. The two-fold uncertainty of the REM estimation (Gattacceca & Rochette, 2004) results in rather large overall uncertainties.

Figures 2g-i shows the PRM acquisition efficiency  $\alpha$ , which compares the PRM to the REM estimate of a TRM. While the PRM is independent of domain-state,  $\alpha$  is not. The large multi-domain sample (16.9  $\mu\text{m}$ ) acquires a PRM that, even at low pressure reaches  $\approx 25\%$  of a full TRM. The smaller grain-sizes, on the other hand acquire "only" 15%, 12% and 10% for the 18.3  $\mu\text{m}$ , 0.44  $\mu\text{m}$  and 0.065  $\mu\text{m}$  samples, respectively. It is well known that the thermal remanence is strongly dependent on the magnetic domain state (Dunlop & Özdemir, 1997). Fine grains (SD, vortex), thereby, acquire a stronger TRM than larger multi-domain grains. Therefore, comparing a grain-size independent PRM with a strongly grain-size dependent TRM will inevitably show such a dependence. Here, the domain-state dependence in  $\alpha$  can be directly related to the saturation remanent magnetization used to estimate the TRM.

Using a similar approach to estimate PRM efficiencies, Tikoo et al. (2015) calculated the ratio (PRM/TRM) after AF-demagnetization at 2 mT ( $\alpha_{2\text{mT}}$ ) for natural samples of various mineralogies.

Our results compare well (fig. 4) with the results for pure magnetite in Gattacceca et al. (2007); Tikoo et al. (2015). However, the pressure used in these studies was a lot higher. Therefore, assuming a continuous increase in  $\alpha$  with pressure, our values are smaller compared to the values reported in (Tikoo et al., 2015). These earlier studies used AF demagnetization (2 mT) to remove any low coercivity viscous magnetizations, which in our study are negligible (i.e.  $M(T_0, P_0)$ ). In the same study Tikoo et al. (2015) found that AF demagnetization is more effective at removing pressure remanence than a thermal remanence. Thus, the smaller values reported by Tikoo et al. (2015) at higher pressures can be explained by this low field AF demagnetization. Regardless, our data confirms the inverse relationship of  $\alpha$  and coercivity or coercivity of remanence. This, shows that while the PRM acquisition is independent of domain state, the efficiency compared to a TRM is not.

## 4.2 Implications

The magnetizations of rocks dominated by single-domain grains should not be affected by PRM overprints, since the PRM efficiency of these grains is low. In contrast, rocks dominated by multi-domain grains, with efficiencies of  $\alpha \approx 25\%$ , may acquire PRMs that are significant relative to their overall remanence. Furthermore, because the PRM overprint would affect large portions of the unblocking spectrum, it may not be easily recognizable. Using the idea that the PRM acquisition is mainly driven by the magnetostriction of a material, it is possible to use the temperature (Moskowitz, 1993) and pressure dependence (Nagata & Kinoshita, 1967) to estimate the changes in PRM magnitude with depth. Figure 3b shows, that when normalized to the room temperature  $\lambda_s$ , PRM acquisition should be less important for high-temperature regimes, such as the greenschist metamorphic facies. On the other hand, in a low-temperature, high-pressure regime, such as the blueschist, and zeolite facies, a PRM overprint of the remanence could be more important.

Magnetostriction increases strongly with the Ti content of magnetite and could result in a much stronger PRM acquisition for Ti-substituted magnetites. This can lead to significantly higher crustal magnetizations when the TRM/PRM is acquired under pressure rather than at ambient pressure (Launay et al., 2017). This could have implications for the interpretation of magnetic anomalies in oceanic crust, where the main magnetic carriers are Ti-magnetite (TM60). The extent to which PRMs will contribute to magnetization in oceanic crust will be moderated by geothermal gradients, which produce Curie depths for TM60 of 5 - 20 km (Li, Lu, & Wang, 2017). More experimental data on PRM acquisition by titanomagnetite are needed to better explore this issue.

Impact processes may also produce scenarios where an original NRM is overprinted by a PRM. While temperature and pressure in the central part of an impact structure can be high enough to melt the surrounding rock, the temperatures of more distal parts of the structure are more moderate (Gilder, Pohl, & Eitel, 2018). The pressure wave generated during an impact extends far beyond this high temperature region to rocks that are cool enough to acquire a PRM. If these rocks are dominated by multi-domain grains, then the resulting PRM may deflect the characteristic remanence direction and confound interpretations of the thermal demagnetization data.

## 5 Conclusions

Our understanding of how rocks acquire magnetization as a function of both temperature and pressure is only in its infancy. A more nuanced understanding of  $M(T,P)$  will ultimately lead to significant advances in the interpretation of magnetic anomalies and impact structures on Earth and other planetary bodies. This study provides a glimpse into the PRM behavior of pure magnetite as a function of grain size across temperatures  $\leq 150^\circ\text{C}$ , but more fundamental research is needed to quantify how pressure alters domain state, blocking and unblocking temperatures, and Curie temperatures for common terrestrial magnetic mineral assemblages. The data reported in this study provide some of the first evidence that PRMs are independent of TRMs at temperatures  $\leq 150^\circ\text{C}$ , yet more research is required to determine if this independence of pressure and thermal remanence persists under the higher temperature/pressure regimes that frequently occur in oceanic and continental crust. PRMs are likely to be more significant in rocks that are dominated by multi-domain grains and are difficult to identify during thermal demagnetization experiments, as PRM unblocking temperatures often extend up to temperatures close to the Curie temperature of magnetite. Thus, more research is also needed to develop tools to unambiguously identify the presence of PRMs. If such progress can be made and the rock magnetic community can isolate the magnetization associated with different stages of a sample's pressure-

temperature history, then we will be able to provide valuable geophysical information for scientists working across a wide range of disciplines, including structural geology, tectonics and geodynamics, and planetary geology.

## 6 Acknowledgments

We would like to thank Mike Jackson and Bruce Moskowitz for valuable discussions on the manuscript. Also, we would like to thank Sonia Tikoo, Nick Swanson-Hysell and Rich Harrison whose comments and suggestions helped improve the manuscript. This work was performed at the Institute for Rock Magnetism (IRM) at the University of Minnesota. The IRM is a US National Multi-user Facility supported through the Instrumentation and Facilities program of the National Science Foundation, Earth Sciences Division, and by funding from the University of Minnesota. All the data used are listed in the references or archived in the database of the Institute for Rock Magnetism ([irm.umn.edu](http://irm.umn.edu)). This is IRM publication (#1816). MWR Volk and JM Feinberg were supported by NSF-EAR-1620582.

## References

- Bezaeva, N. S., Gattacceca, J., Rochette, P., Sadykov, R. A., & Trukhin, V. I. (2010, mar). Demagnetization of terrestrial and extraterrestrial rocks under hydrostatic pressure up to 1.2GPa. *Phys. Earth Planet. Inter.*, *179*(1-2), 7–20. Retrieved from <http://linkinghub.elsevier.com/retrieve/pii/S0031920110000075> doi: 10.1016/j.pepi.2010.01.004
- Bickford, L. R., Pappis, J., & Stull, J. L. (1955). Magnetostriction and permeability of magnetite and cobalt-substituted magnetite. *Physical Review*, *99*(4), 1210–1214. doi: 10.1103/PhysRev.99.1210
- Carter-Stiglitz, B., Moskowitz, B. M., Solheid, P. A., Berquó, T. S., Jackson, M. J., & Kosterov, A. A. (2006). Low-temperature magnetic behavior of multidomain titanomagnetites: TM0, TM16, and TM35. *J. Geophys. Res. Solid Earth*, *111*(B12), n/a—n/a. Retrieved from <http://doi.wiley.com/10.1029/2006JB004561> doi: 10.1029/2006JB004561
- Day, R., Fuller, M. D., & Schmidt, V. a. (1977). Hysteresis properties of titanomagnetites: Grain-size and compositional dependence. *Phys. Earth Planet. Inter.*, *13*(4), 260–267. Retrieved from <http://linkinghub.elsevier.com/retrieve/pii/003192017790108X> doi: 10.1016/0031-9201(77)90108-X
- Dunlop, D. J. (2002). Theory and application of the Day plot (Mrs/Ms versus Hcr/Hc) 1. Theoretical curves and tests using titanomagnetite data. *Journal of Geophysical Research*, *107*(B3), EPM4–1 – EPM4–22. Retrieved from <http://www.agu.org/pubs/crossref/2002/2001JB000486.shtml> doi: 10.1029/2001JB000486
- Dunlop, D. J., & Özdemir, Ö. (1997). *Rock Magnetism*. Cambridge: Cambridge University Press. Retrieved from <http://ebooks.cambridge.org/ref/id/CB09780511612794> doi: 10.1017/CBO9780511612794
- Egli, R. (2013). VARIFORC: An optimized protocol for calculating non-regular first-order reversal curve (FORC) diagrams. *Global and Planetary Change*, *110*, 302–320. Retrieved from <http://www.sciencedirect.com/science/article/pii/S0921818113001744> doi: 10.1016/j.gloplacha.2013.08.003
- Fabian, K. (2006). Approach to saturation analysis of hysteresis measurements in rock magnetism and evidence for stress dominated magnetic anisotropy in young mid-ocean ridge basalt. *Phys. Earth Planet. Inter.*, *154*(3-4), 299–307. Retrieved from <http://linkinghub.elsevier.com/retrieve/pii/S0031920105002633> doi: 10.1016/j.pepi.2005.06.016
- Fabian, K., Shcherbakov, V. P., & McEnroe, S. A. (2013). Measuring the Curie temperature. *Geochemistry, Geophysics, Geosystems*, *14*(4), 947–961. Re-

- trieved from <http://doi.wiley.com/10.1029/2012GC004440> doi: 10.1029/2012GC004440
- Gattacceca, J., Lamali, A., Rochette, P., Boustie, M., & Berthe, L. (2007). The effects of explosive-driven shocks on the natural remanent magnetization and the magnetic properties of rocks. *Phys. Earth Planet. Inter.*, *162*(1), 85–98. Retrieved from <http://www.sciencedirect.com/science/article/pii/S0031920107000581> doi: 10.1016/j.pepi.2007.03.006
- Gattacceca, J., & Rochette, P. (2004, November). Toward a robust normalized magnetic paleointensity method applied to meteorites. *Earth and Planetary Science Letters*, *227*(3-4), 377–393.
- Gilder, S. A., & Le Goff, M. (2008). Systematic pressure enhancement of titanomagnetite magnetization. *Geophys. Res. Lett.*, *35*(10), L10302. Retrieved from <http://doi.wiley.com/10.1029/2008GL033325> doi: 10.1029/2008GL033325
- Gilder, S. A., Pohl, J., & Eitel, M. (2018). Magnetic Signatures of Terrestrial Meteorite Impact Craters: A Summary BT - Magnetic Fields in the Solar System: Planets, Moons and Solar Wind Interactions. In H. Lühr, J. Wicht, S. A. Gilder, & M. Holschneider (Eds.), (pp. 357–382). Cham: Springer International Publishing. Retrieved from [https://doi.org/10.1007/978-3-319-64292-5\\_{\\\_}13](https://doi.org/10.1007/978-3-319-64292-5_{\_}13) doi: 10.1007/978-3-319-64292-5\_13
- Gillen, C. (1982). *Metamorphic Geology*. Dordrecht: Springer Netherlands. Retrieved from <http://link.springer.com/10.1007/978-94-011-5978-4> doi: 10.1007/978-94-011-5978-4
- Harrison, R. J., & Feinberg, J. M. (2008). FORCinel: An improved algorithm for calculating first-order reversal curve distributions using locally weighted regression smoothing. *Geochemistry, Geophys. Geosystems*, *9*(5), n/a—n/a. Retrieved from <http://doi.wiley.com/10.1029/2008GC001987> doi: 10.1029/2008GC001987
- Harrison, R. J., & Lascu, I. (2014, dec). FORCulator: A micromagnetic tool for simulating first-order reversal curve diagrams. *Geochemistry, Geophysics, Geosystems*, *15*(12), 4671–4691. Retrieved from <http://doi.wiley.com/10.1002/2014GC005582> doi: 10.1002/2014GC005582
- Hazen, R. M. (1985). Chapter 9. Comparative Crystal Chemistry and the Polyhedral Approach. In *Reviews in mineralogy volume 14: Microscopic to macroscopic* (pp. 317–346). Mineralogical Society of America. doi: 10.1515/9781501508868-011
- Kinoshita, H. (1968a). Studies on Piezo-Magnetization (II). *J. Geomagn. Geoelectr.*, *20*(2), 75–83. Retrieved from <http://joi.jlc.jst.go.jp/JST.Journalarchive/jgg1949/20.75?from=CrossRef> doi: 10.5636/jgg.20.75
- Kinoshita, H. (1968b). Studies on Piezo-Magnetization (III). *J. Geomagn. Geoelectr.*, *20*(3), 155–167. Retrieved from <http://joi.jlc.jst.go.jp/JST.Journalarchive/jgg1949/20.155?from=CrossRef> doi: 10.5636/jgg.20.155
- Kinoshita, H. (1969). Studies on Piezo-Magnetization (IV). *J. Geomagn. Geoelectr.*, *21*(1), 409–426. Retrieved from <http://joi.jlc.jst.go.jp/JST.Journalarchive/jgg1949/21.409?from=CrossRef> doi: 10.5636/jgg.21.409
- Kinoshita, H., & Nagata, T. (1967). Dependence of Magnetostriction and Magnetocrystalline Anisotropy of Magnetite on Hydrostatic Pressure. *J. Geomagn. Geoelectr.*, *19*(1), 77–79. doi: 10.5636/jgg.19.77
- Kletetschka, G., Kohout, T., & Wasilewski, P. J. (2003). Magnetic remanence in the Murchison meteorite. *Meteoritics & Planetary Science*, *38*(3), 399–405.
- Kontny, A., Reznik, B., Boubnov, A., Göttlicher, J., & Steininger, R. (2018). Post-Shock Thermally Induced Transformations in Experimentally Shocked Magnetite. *Geochemistry, Geophys. Geosystems*, *42*(1), 93. Retrieved from <https://agupubs.onlinelibrary.wiley.com/doi/full/10.1002/2017GC007331> doi: 10.1002/2017GC007331

- Launay, N., Rochette, P., Quesnel, Y., Demory, F., Bezaeva, N. S., & Lattard, D. (2017). Thermoremanence acquisition and demagnetization for titanomagnetite under lithospheric pressures. *Geophys. Res. Lett.*, *44*(10), 4839–4845. Retrieved from <http://doi.wiley.com/10.1002/2017GL073279> doi: 10.1002/2017GL073279
- Li, C.-F., Lu, Y., & Wang, J. (2017, dec). A global reference model of Curie-point depths based on EMAG2. *Scientific Reports*, *7*(1), 45129. Retrieved from <http://www.nature.com/articles/srep45129> doi: 10.1038/srep45129
- Lindquist, A. K., Feinberg, J. M., Harrison, R. J., Loudon, J. C., & Newell, A. J. (2015, mar). Domain wall pinning and dislocations: Investigating magnetite deformed under conditions analogous to nature using transmission electron microscopy. *Journal of Geophysical Research: Solid Earth*, *120*(3), 1415–1430. Retrieved from <http://doi.wiley.com/10.1002/2014JB011335> doi: 10.1002/2014JB011335
- Liu, Q., Jackson, M. J., Banerjee, S. K., Zhu, R., Pan, Y., & Chen, F. (2003). Determination of magnetic carriers of the characteristic remanent magnetization of Chinese loess by low-temperature demagnetization. *Earth Planet. Sci. Lett.*, *216*(1-2), 175–186. Retrieved from <http://linkinghub.elsevier.com/retrieve/pii/S0012821X03004771> doi: 10.1016/S0012-821X(03)00477-1
- Louzada, K. L., Stewart, S. T., Weiss, B. P., Gattacceca, J., & Bezaeva, N. S. (2010). Shock and static pressure demagnetization of pyrrhotite and implications for the Martian crust. *Earth Planet. Sci. Lett.*, *290*(1-2), 90–101. Retrieved from <http://linkinghub.elsevier.com/retrieve/pii/S0012821X09007298> doi: 10.1016/j.epsl.2009.12.006
- Louzada, K. L., Stewart, S. T., Weiss, B. P., Gattacceca, J., Lillis, R. J., & Halekas, J. S. (2011). Impact demagnetization of the Martian crust: Current knowledge and future directions. *Earth Planet. Sci. Lett.*, *305*(3-4), 257–269. Retrieved from <http://www.sciencedirect.com/science/article/pii/S0012821X11001579> doi: 10.1016/j.epsl.2011.03.013
- Moskowitz, B. M. (1993). High-temperature magnetostriction of magnetite and titanomagnetites. *J. Geophys. Res. Solid Earth*, *98*(B1), 359–371. Retrieved from <http://doi.wiley.com/10.1029/92JB01846> doi: 10.1029/92JB01846
- Nagata, T. (1966). Main Characteristics of Piezo-Magnetization and Their Qualitative Interpretation. *J. Geomagn. Geoelectr.*, *18*(1), 81–97. Retrieved from <http://joi.jlc.jst.go.jp/JST.Journalarchive/jgg1949/18.81?from=CrossRef> doi: 10.5636/jgg.18.81
- Nagata, T., & Carleton, B. J. (1968). Notes on Piezo-remnant Magnetization of Igneous Rocks. *J. Geomagn. Geoelectr.*, *20*(3), 115–127. Retrieved from <http://joi.jlc.jst.go.jp/JST.Journalarchive/jgg1949/20.115?from=CrossRef> doi: 10.5636/jgg.20.115
- Nagata, T., & Carleton, B. J. (1969a). Notes on Piezo-remnant Magnetization of Igneous Rocks II. *J. Geomagn. Geoelectr.*, *21*(1), 427–445. Retrieved from <http://joi.jlc.jst.go.jp/JST.Journalarchive/jgg1949/21.427?from=CrossRef> doi: 10.5636/jgg.21.427
- Nagata, T., & Carleton, B. J. (1969b). Notes on Piezo-remnant Magnetization of Igneous Rocks III. *J. Geomagn. Geoelectr.*, *21*(3), 623–645. Retrieved from <http://joi.jlc.jst.go.jp/JST.Journalarchive/jgg1949/21.623?from=CrossRef> doi: 10.5636/jgg.21.623
- Nagata, T., & Kinoshita, H. (1965). Studies on Piezo-Magnetization (I). *J. Geomagn. Geoelectr.*, *17*(2), 121–135. Retrieved from <http://joi.jlc.jst.go.jp/JST.Journalarchive/jgg1949/17.121?from=CrossRef> doi: 10.5636/jgg.17.121
- Nagata, T., & Kinoshita, H. (1967). Effect of hydrostatic pressure on magnetostriction and magnetocrystalline anisotropy of magnetite. *Phys. Earth Planet. Inter.*, *1*(1), 44–48. Retrieved from <http://linkinghub.elsevier.com/>

- retrieve/pii/0031920167900076 doi: 10.1016/0031-9201(67)90007-6
- Özdemir, Ö., Dunlop, D. J., & Moskowitz, B. M. (1993). The effect of oxidation on the Verwey transition in magnetite. *Geophys. Res. Lett.*, *20*(16), 1671–1674. doi: 10.1029/93gl01483
- Petrovský, E., & Kapička, A. (2006, dec). On determination of the Curie point from thermomagnetic curves. *Journal of Geophysical Research: Solid Earth*, *111*(B12). Retrieved from <http://doi.wiley.com/10.1029/2006JB004507> doi: 10.1029/2006JB004507
- Reznik, B., Kontny, A., Fritz, J., & Gerhards, U. (2016). Shock-induced deformation phenomena in magnetite and their consequences on magnetic properties. *Geochemistry, Geophys. Geosystems*, *17*(6), 2374–2393. Retrieved from <http://doi.wiley.com/10.1002/2016GC006338> doi: 10.1002/2016GC006338
- Roberts, A. P., Heslop, D., Zhao, X., & Pike, C. R. (2014). Understanding fine magnetic particle systems through use of first-order reversal curve diagrams. *Rev. Geophys.*, *52*(4), 557–602. Retrieved from <http://doi.wiley.com/10.1002/2014RG000462> doi: 10.1002/2014RG000462
- Shepherd, J. P., Koenitzer, J. W., Aragn, R., Spalek, J., & Honig, J. M. (1991, apr). Heat capacity and entropy of nonstoichiometric magnetite Fe<sub>3</sub>(1-x)O<sub>4</sub>: The thermodynamic nature of the Verwey transition. *Phys. Rev. B*, *43*(10), 8461–8471. Retrieved from <https://link.aps.org/doi/10.1103/PhysRevB.43.8461> doi: 10.1103/PhysRevB.43.8461
- Stöffler, D., Keil, K., & Edward R D, S. (1991). Shock metamorphism of ordinary chondrites. *Geochim. Cosmochim. Acta*, *55*(12), 3845–3867. Retrieved from <http://linkinghub.elsevier.com/retrieve/pii/001670379190078J> doi: 10.1016/0016-7037(91)90078-J
- Tikoo, S. M., Gattacceca, J., Swanson-Hysell, N. L., Weiss, B. P., Suavet, C., & Cournède, C. (2015, September). Preservation and detectability of shock-induced magnetization. *Journal of Geophysical Research: Planets*, *120*(9), 1461–1475.
- Tikoo, S. M., Weiss, B. P., Cassata, W. S., Shuster, D. L., Gattacceca, J. Ô., Lima, E. A., . . . Fuller, M. D. (2014). Decline of the lunar core dynamo. *Earth Planet. Sci. Lett.*, *404*, 89–97. Retrieved from <http://dx.doi.org/10.1016/j.epsl.2014.07.010> doi: 10.1016/j.epsl.2014.07.010
- Verwey, E. J. (1939). Electronic conduction of magnetite (Fe<sub>3</sub>O<sub>4</sub>) and its transition point at low temperatures. *Nature*, *144*(3642), 327–328. Retrieved from <http://www.nature.com/doi/10.1038/144327b0> doi: 10.1038/144327b0
- Volk, M. W., & Gilder, S. A. (2016). Effect of static pressure on absolute paleointensity recording with implications for meteorites. *J. Geophys. Res. Solid Earth*, *121*(8), 5596–5610. Retrieved from <http://doi.wiley.com/10.1002/2016JB013059> doi: 10.1002/2016JB013059
- Wang, D., & Van der Voo, R. (2004). The hysteresis properties of multidomain magnetite and titanomagnetite/titanomaghemite in mid-ocean ridge basalts. *Earth Planet. Sci. Lett.*, *220*(1-2), 175–184. Retrieved from <http://linkinghub.elsevier.com/retrieve/pii/S0012821X04000524> doi: 10.1016/S0012-821X(04)00052-4
- Yu, Y., Dunlop, D. J., & Özdemir, Ö. (2002, October). Partial anhysteretic remanent magnetization in magnetite 1. Additivity. *Journal of Geophysical Research: Solid Earth*, *107*(B10), EPM 7–1–EPM 7–9.
- Yu, Y., Dunlop, D. J., & Özdemir, Ö. (2002). Partial anhysteretic remanent magnetization in magnetite 2. Reciprocity. *Journal of Geophysical Research: Solid Earth*, *107*(B10), EPM 8—1—EPM 8—9. Retrieved from <http://www.agu.org/pubs/crossref/2002/2001JB001269.shtml> doi: 10.1029/2001JB001269